Project 1: Yee vs. UCHIE

Yens Lindemans (yens.lindemans@ugent.be)
Daan Verraes (daan.verraes@ugent.be)

Multiscale and Multiphysics Modeling Technique for Nanoelectronic Devices
Elective Course Master of Engineering Physics
Faculty of Engineering and Architecture
Ghent University
2023

1 Methodology

1.1 Continuous equations

In the 2-D setting imposed by the assignment, the transversal magnetic (TM) mode concerns the following electric and magnetic field components:

$$\mathbf{e}(x,y,t) = e_z(x,y,t)\mathbf{u}_z \tag{1}$$
$$\mathbf{h}(x,y,t) = h_x(x,y,t)\mathbf{u}_x + h_y(x,y,t)\mathbf{u}_y \tag{2}$$

These field components are governed by Maxwell's 2-D TM curl equations:

$$\frac{\partial e_z}{\partial x} = \frac{\partial}{\partial t}(\mu_0\mu_r h_y) \tag{3}$$
$$\frac{\partial e_z}{\partial y} = -\frac{\partial}{\partial t}(\mu_0\mu_r h_x) \tag{4}$$
$$\frac{\partial h_y}{\partial x} - \frac{\partial h_x}{\partial y} = \frac{\partial}{\partial t}(\epsilon_0\epsilon_r e_z) + \sigma e_z + j_{e,z} \tag{5}$$

The implementation of perfectly matching layers (PML) at the boundaries of the simulation domain together with the option to add Drude materials give rise to the following set of equations:

$$\frac{\partial e_z}{\partial x} = \mu\frac{\partial \dot{h}_y}{\partial t} \tag{6}$$
$$\kappa_x\frac{\partial h_y}{\partial t} + \frac{\sigma_x}{\epsilon}h_y = \kappa_y\frac{\partial \dot{h}_y}{\partial t} + \frac{\sigma_y}{\epsilon}\dot{h}_y \tag{7}$$
$$-\frac{\partial e_z}{\partial y} = \mu\kappa_y\frac{\partial \dot{h}_x}{\partial t} + \mu\frac{\sigma_y}{\epsilon}\dot{h}_x \tag{8}$$
$$\frac{\partial h_x}{\partial t} = \kappa_x\frac{\partial \dot{h}_x}{\partial t} + \frac{\sigma_x}{\epsilon}\dot{h}_x \tag{9}$$
$$\frac{\partial h_y}{\partial x} - \frac{\partial h_x}{\partial y} = \epsilon\frac{\partial \ddot{e}_z}{\partial t} + j_{c,z} + j_{e,z} \tag{10}$$
$$\kappa_y\frac{\partial e_z}{\partial t} + \frac{\sigma_y}{\epsilon}e_z = \frac{\partial \dot{e}_z}{\partial t} \tag{11}$$
$$\gamma\frac{\partial j_{c,z}}{\partial t} + j_{c,z} = \sigma_{DC}\ddot{e}_z \tag{12}$$
$$\kappa_x\frac{\partial \dot{e}_z}{\partial t} + \frac{\sigma_x}{\epsilon}\dot{e}_z = \frac{\partial \ddot{e}_z}{\partial t} \tag{13}$$

where the auxiliary fields $\dot{h}_y$, $\dot{e}_z$, $\ddot{e}_z$ and $\dot{h}_x$ are added to model the dispersive PML, described by κ_x, σ_x, κ_y and σ_y and the Drude media, described by σ_{DC} and γ.

1.2 2-D TM UCHIE scheme

In the 2-D unidirectionally collocated FDTD scheme, the field components are collocated along one direction, here the x-direction, and staggered in the other direction. The 2-D TM fields are then discretized as follows:

$$e_z|_{i,j}^{n+\frac{1}{2}} = e_z(i\Delta x, j\Delta y, (n+\frac{1}{2})\Delta t) \tag{14}$$

$$h_y|_{i,j}^{n+\frac{1}{2}} = h_y(i\Delta x, j\Delta y, (n+\frac{1}{2})\Delta t) \tag{15}$$

$$h_x|_{i,j+\frac{1}{2}}^{n} = h_x(i\Delta x, (j+\frac{1}{2})\Delta y, n\Delta t) \tag{16}$$

where the h_x field is also staggered in time w.r.t. the e_z and h_y fields. The auxiliary fields are discretized the same way as their respective physical fields.
The 2-D unidirectionally collocated cells with the field components as discussed above can be seen in figure 1.

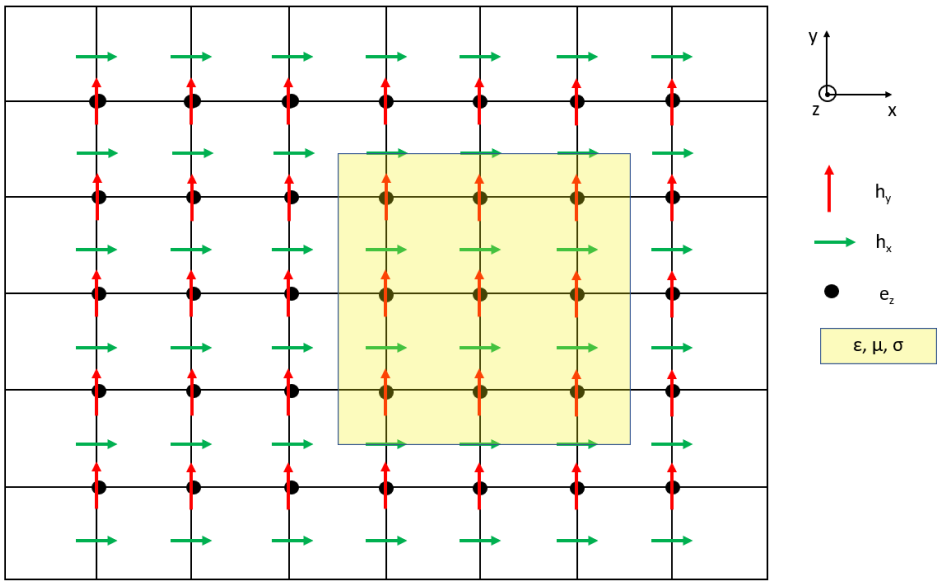

Figure 1: The unidirectionally collocated cell with the field components of the 2-D TM problem. The material boundaries are located on dual grid cell boundaries (*i.e.* at $i+\frac{1}{2}$ and $j+\frac{1}{2}$)

Here, every material boundary is located on dual grid cell boundaries (*i.e.* at $i+\frac{1}{2}$ and $j+\frac{1}{2}$), which is a first advantage of this scheme as discussed later.

1.3 Update equations

Discretizing equations 8 and 9 according to the UCHIE FDTD method then leads to the following explicit update equations:

$$\left(\frac{\bar{\mu}\bar{\kappa}_y}{\Delta t} + \bar{\mu}\frac{\bar{\sigma}_y}{2\bar{\epsilon}}\right)\dot{h}_x\Big|_{i,j+\frac{1}{2}}^{n+1} = \left(\frac{\bar{\mu}\bar{\kappa}_y}{\Delta t} - \bar{\mu}\frac{\bar{\sigma}_y}{2\bar{\epsilon}}\right)\dot{h}_x\Big|_{i,j+\frac{1}{2}}^{n} - \frac{1}{\Delta y}\left(e_z|_{i,j+1}^{n+\frac{1}{2}} - e_z|_{i,j}^{n+\frac{1}{2}}\right) \tag{17}$$

$$h_x|_{i,j+\frac{1}{2}}^{n+1} = h_x|_{i,j+\frac{1}{2}}^{n} + \left(\bar{\kappa}_x + \frac{\bar{\sigma}_x}{2\bar{\epsilon}}\Delta t\right)\dot{h}_x\Big|_{i,j+\frac{1}{2}}^{n+1} - \left(\bar{\kappa}_x - \frac{\bar{\sigma}_x}{2\bar{\epsilon}}\Delta t\right)\dot{h}_x\Big|_{i,j+\frac{1}{2}}^{n} \tag{18}$$

where it is important to note that the material parameters on the horizontal material boundaries (at $j+\frac{1}{2}$) should be interpolated using the (non-uniform) grid step sizes near the boundaries in the y-direction as weighting, hence the bars. The other equations (6, 7, 10, 11, 12 and 13) result (using adequate interpolations of the fields) in the following implicit update equations:

$$\frac{\mu}{\Delta t}\left(\dot{h}_y\Big|_{i,j}^{n+\frac{1}{2}}+\dot{h}_y\Big|_{i+1,j}^{n+\frac{1}{2}}\right)-\frac{1}{\Delta x}\left(e_z|_{i+1,j}^{n+\frac{1}{2}}-e_z|_{i,j}^{n+\frac{1}{2}}\right)=\frac{\mu}{\Delta t}\left(\dot{h}_y\Big|_{i,j}^{n-\frac{1}{2}}+\dot{h}_y\Big|_{i+1,j}^{n-\frac{1}{2}}\right)+\frac{1}{\Delta x}\left(e_z|_{i+1,j}^{n-\frac{1}{2}}-e_z|_{i,j}^{n-\frac{1}{2}}\right) \tag{19}$$

$$-\left(\frac{\kappa_y}{\Delta t}+\frac{\sigma_y}{2\epsilon}\right)\dot{h}_y\Big|_{i,j}^{n+\frac{1}{2}}+\left(\frac{\kappa_x}{\Delta t}+\frac{\sigma_x}{2\epsilon}\right)h_y|_{i,j}^{n+\frac{1}{2}}=-\left(\frac{\kappa_y}{\Delta t}-\frac{\sigma_y}{2\epsilon}\right)\dot{h}_y\Big|_{i,j}^{n-\frac{1}{2}}+\left(\frac{\kappa_x}{\Delta t}-\frac{\sigma_x}{2\epsilon}\right)h_y|_{i,j}^{n-\frac{1}{2}} \tag{20}$$

$$\begin{aligned}&\frac{\epsilon}{\Delta t}\left(\ddot{e}_z|_{i,j}^{n+\frac{1}{2}}+\ddot{e}_z|_{i+1,j}^{n+\frac{1}{2}}\right)-\frac{1}{\Delta x}\left(h_y|_{i+1,j}^{n+\frac{1}{2}}-h_y|_{i,j}^{n+\frac{1}{2}}\right)+\frac{1}{2}\left(j_{c,z}|_{i+1,j}^{n+\frac{1}{2}}+j_{c,z}|_{i,j}^{n+\frac{1}{2}}\right)\\ =&\frac{\epsilon}{\Delta t}\left(\ddot{e}_z|_{i,j}^{n-\frac{1}{2}}+\ddot{e}_z|_{i+1,j}^{n-\frac{1}{2}}\right)+\frac{1}{\Delta x}\left(h_y|_{i+1,j}^{n-\frac{1}{2}}-h_y|_{i,j}^{n-\frac{1}{2}}\right)-\frac{1}{2}\left(j_{c,z}|_{i+1,j}^{n-\frac{1}{2}}+j_{c,z}|_{i,j}^{n-\frac{1}{2}}\right)\\ &-\frac{1}{\Delta y^*}\left(h_x|_{i+1,j+\frac{1}{2}}^{n}-h_x|_{i+1,j-\frac{1}{2}}^{n}+h_x|_{i,j+\frac{1}{2}}^{n}-h_x|_{i,j-\frac{1}{2}}^{n}\right)-2j_{e,z}\end{aligned} \tag{21}$$

$$-\frac{1}{\Delta t}\,\dot{e}_z|_{i,j}^{n+\frac{1}{2}}+\left(\frac{\kappa_y}{\Delta t}+\frac{\sigma_y}{2\epsilon}\right)e_z|_{i,j}^{n+\frac{1}{2}}=-\frac{1}{\Delta t}\,\dot{e}_z|_{i,j}^{n-\frac{1}{2}}+\left(\frac{\kappa_y}{\Delta t}-\frac{\sigma_y}{2\epsilon}\right)e_z|_{i,j}^{n-\frac{1}{2}} \tag{22}$$

$$\left(\frac{2\gamma}{\Delta t}+1\right)j_{c,z}|_{1,j}^{n+\frac{1}{2}}-\sigma_{DC}\,\ddot{e}_z|_{i,j}^{n+\frac{1}{2}}=\left(\frac{2\gamma}{\Delta t}-1\right)j_{c,z}|_{1,j}^{n-\frac{1}{2}}+\sigma_{DC}\,\ddot{e}_z|_{i,j}^{n-\frac{1}{2}} \tag{23}$$

$$-\frac{1}{\Delta t}\,\ddot{e}_z|_{i,j}^{n+\frac{1}{2}}+\left(\frac{\kappa_x}{\Delta t}+\frac{\sigma_x}{2\epsilon}\right)\dot{e}_z|_{i,j}^{n+\frac{1}{2}}=-\frac{1}{\Delta t}\,\ddot{e}_z|_{i,j}^{n-\frac{1}{2}}+\left(\frac{\kappa_x}{\Delta t}-\frac{\sigma_x}{2\epsilon}\right)\dot{e}_z|_{i,j}^{n-\frac{1}{2}} \tag{24}$$

Note that the interpolations of the fields in these implicit equations do not demand interpolations of material parameters, but the correct parameters should be used at the relevant field components (see later). The implicit update equations can be written in matrix notation for every j-index as:

$$M_j.x_j^{n+\frac{1}{2}}=N_j.x_j^{n-\frac{1}{2}}+b_j^n \tag{25}$$

with

$$M_j=\begin{bmatrix}\left[\frac{2\gamma}{\Delta t}+1\right] & -[\sigma_{DC}] & 0 & 0 & 0 & 0\\ \frac{A_I}{2} & \frac{A_I}{\Delta t}[\epsilon] & 0 & 0 & -\frac{1}{\Delta x}A_D & 0\\ 0 & 0 & \frac{A_I}{\Delta t}[\mu] & 0 & 0 & -\frac{1}{\Delta x}A_D\\ 0 & -\frac{1}{\Delta t} & 0 & \left[\frac{\kappa_x}{\Delta t}+\frac{\sigma_x}{2\epsilon}\right] & 0 & 0\\ 0 & 0 & -\left[\frac{\kappa_y}{\Delta t}+\frac{\sigma_y}{2\epsilon}\right] & 0 & \left[\frac{\kappa_x}{\Delta t}+\frac{\sigma_x}{2\epsilon}\right] & 0\\ 0 & 0 & 0 & -\frac{1}{\Delta t} & 0 & \left[\frac{\kappa_y}{\Delta t}+\frac{\sigma_y}{2\epsilon}\right]\end{bmatrix} \tag{26}$$

$$N_j=\begin{bmatrix}\left[\frac{2\gamma}{\Delta t}-1\right] & [\sigma_{DC}] & 0 & 0 & 0 & 0\\ -\frac{A_I}{2} & \frac{A_I}{\Delta t}[\epsilon] & 0 & 0 & \frac{1}{\Delta x}A_D & 0\\ 0 & 0 & \frac{A_I}{\Delta t}[\mu] & 0 & 0 & \frac{1}{\Delta x}A_D\\ 0 & -\frac{1}{\Delta t} & 0 & \left[\frac{\kappa_x}{\Delta t}-\frac{\sigma_x}{2\epsilon}\right] & 0 & 0\\ 0 & 0 & -\left[\frac{\kappa_y}{\Delta t}-\frac{\sigma_y}{2\epsilon}\right] & 0 & \left[\frac{\kappa_x}{\Delta t}-\frac{\sigma_x}{2\epsilon}\right] & 0\\ 0 & 0 & 0 & -\frac{1}{\Delta t} & 0 & \left[\frac{\kappa_y}{\Delta t}-\frac{\sigma_y}{2\epsilon}\right]\end{bmatrix} \tag{27}$$

$$x_j^{n+\frac{1}{2}} = \begin{bmatrix} \dot{j}_{c,z}\big|_{0,j}^{n+\frac{1}{2}} \\ \vdots \\ \dot{j}_{c,z}\big|_{N_x-1,j}^{n+\frac{1}{2}} \\ \vdots \\ \ddot{e}_z\big|_{0,j}^{n+\frac{1}{2}} \\ \vdots \\ \ddot{e}_z\big|_{N_x-1,j}^{n+\frac{1}{2}} \\ \dot{h}_y\Big|_{0,j}^{n+\frac{1}{2}} \\ \vdots \\ \dot{h}_y\Big|_{N_x-1,j}^{n+\frac{1}{2}} \\ \dot{e}_z\big|_{0,j}^{n+\frac{1}{2}} \\ \vdots \\ \dot{e}_z\big|_{N_x-1,j}^{n+\frac{1}{2}} \\ h_y\big|_{0,j}^{n+\frac{1}{2}} \\ \vdots \\ h_y\big|_{N_x-1,j}^{n+\frac{1}{2}} \\ e_z\big|_{0,j}^{n+\frac{1}{2}} \\ \vdots \\ e_z\big|_{N_x-1,j}^{n+\frac{1}{2}} \end{bmatrix} \tag{28}$$

$$b_j^n = -\begin{bmatrix} 0 \\ \frac{A_I}{\Delta y^*}(\,h_x|_{i,j+\frac{1}{2}}^n - h_x|_{i,j-\frac{1}{2}}^n) + 2j_{e,z} \\ 0 \\ 0 \\ 0 \\ 0 \end{bmatrix} \tag{29}$$

where the material parameters μ, ϵ, σ_{DC}, γ, κ_x, σ_x, κ_y and σ_y are represented by $m \times m$ diagonal matrices at every y-step j (hence the square brackets), so that they are assigned to the correct field component. The interpolation operator A_I and differential operator A_D are $m \times m$ matrices defined as:

$$A_I = \begin{bmatrix} 1 & 1 & 0 & 0 & \dots \\ 0 & 1 & 1 & 0 & \dots \\ \vdots & \vdots & \vdots & \vdots & \ddots \\ 1 & 0 & \dots & 0 & 1 \end{bmatrix} \tag{30}$$

$$A_D = \begin{bmatrix} -1 & 1 & 0 & 0 & \dots \\ 0 & -1 & 1 & 0 & \dots \\ \vdots & \vdots & \vdots & \vdots & \ddots \\ 1 & 0 & \dots & 0 & -1 \end{bmatrix} \tag{31}$$

The operators are chosen in this form to incorporate periodic boundary conditions (PBC).

2 Results

This section discusses some results of the UCHIE FDTD and compares the scheme with both Yee and analytical solutions. Note that spatial coordinates are written as (x, y), where the units are often omitted, but are assumed to be in meter.

2.1 Validation in free space

2.1.1 Comparison with analytical result

The electric field emitted by a sinusoidal line source in free space is analytically known and is given by equation 10 of the assignment. This result can be used to validate the UCHIE FDTD method in free space, but simulating a sinusoidal source gives a rather poor bandwidth (an impulse on the central frequency), so the frequency response z_z was compared instead:

$$z_z(x, y, \omega) = \frac{e_z(x, y, \omega)}{J_{e,z}(x, y, \omega)} \tag{32}$$

Here, the spectrum of the electric field $e_z(x, y, \omega)$ is a result of a source with current spectrum $J_{e,z}(x, y, \omega)$ being a modulated Gaussian, with a bandwidth and central frequency in the wanted frequency range as seen in figure 2.

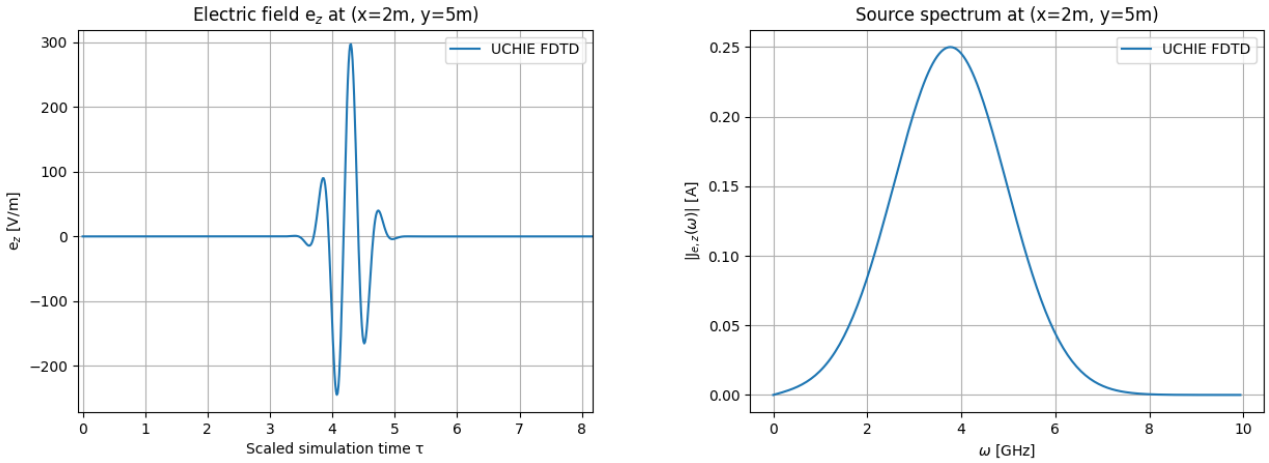

Figure 2: The electric field $e_z(x, y, \omega)$ measured at position (2, 5) (left figure) corresponding to a line source at position (2, 2) with spectrum of the current $J_{e,z}(x, y, \omega)$ being a modulated Gaussian pulse with a central frequency of 3.77 GHz, a Gaussian width of 0.83ns and an amplitude of 2A (right figure).

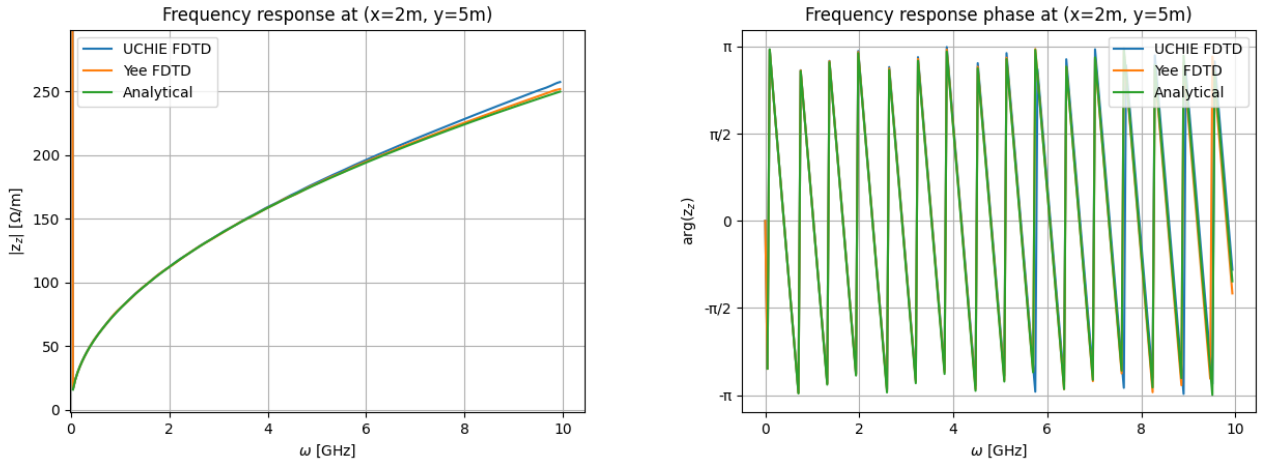

Figure 3: Comparison of the frequency response at (2, 5) of a line source located at (2, 2) between the analytical and simulated results (both Yee and UCHIE FDTD). Left figure shows the absolute value of the response and right figure shows the phase.

A comparison of the absolute value and phase of eq. 32 can be seen in figure 3. Note that for high frequencies, the absolute value of the response starts to deviate from the analytical result, which is due to numerical errors and the fact that these frequencies are outside the bandwidth of the source. The phase, shown in the figure on the right, also deviates from the analytical result for high frequencies. The reason for this is the same as for the absolute value as well as due to the numerical dispersion error. A finer discretization Δx, Δy gives a more accurate phase for higher frequencies. For lower frequencies, the numerical simulation follows the analytical solution.

2.1.2 Comparison with Yee FDTD

As a first comparison of the UCHIE and Yee FDTD schemes, the free propagation for different sources is simulated for both schemes. The resulting fields after free propagation is plotted in

figure 4 for a Gaussian pulse and a modulated Gaussian pulse with amplitude 2 A. The figure shows that both schemes give the same result in this case.

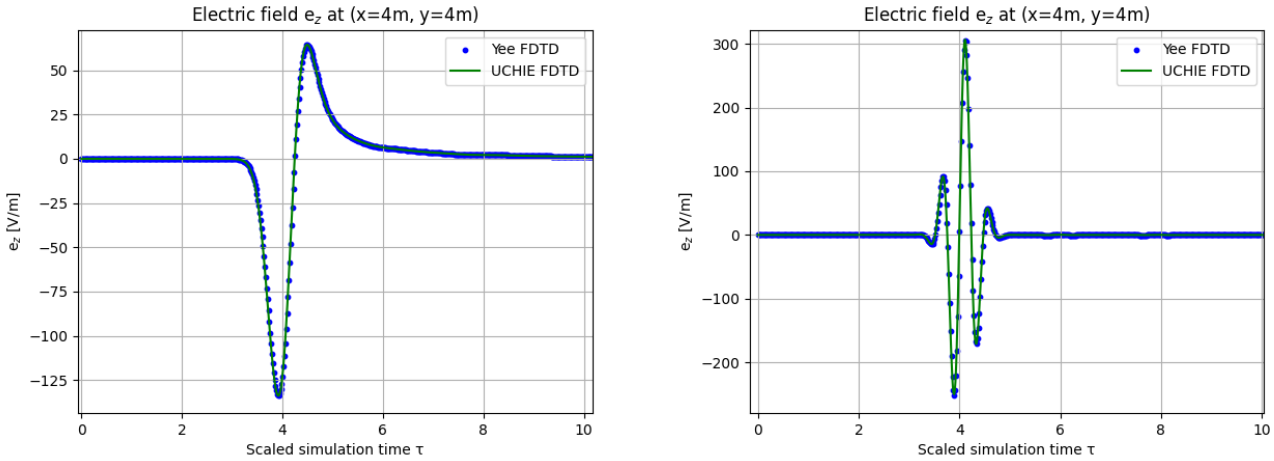

Figure 4: The electric fields $e_z(x, y, \omega)$ at (4,4) simulated using Yee and UCHIE FDTD corresponding to a line source at (2, 2) with spectrum of the current $J_{e,z}(x, y, \omega)$ being a Gaussian pulse (left figure) and a modulated Gaussian pulse with a central frequency of 3.77 GHz (right figure).

2.2 Scattering at dielectric objects

The following comparison with Yee FDTD is for the scattering at dielectric objects as sketched in figure 1. The reflected and transmitted electric fields at (2, 4) and (5, 2) respectively for a Gaussian source and a modulated Gaussian source at (2, 2) and a dielectric material confined in the area $\{x \in [3, 4], y \in [1, 4]\}$ with a relative permittivity $\epsilon_r = 3$ can be seen in figure 5 and 6 respectively. Again, Yee and UCHIE FTDT give a very similar result.

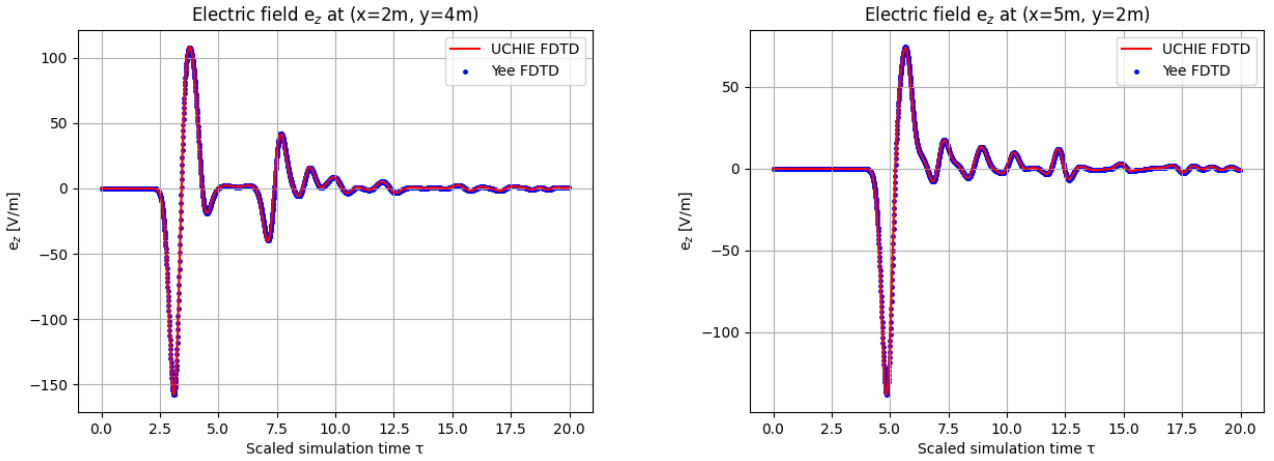

Figure 5: The electric fields $e_z(x, y, \omega)$ at (2,4) (left figure) and (5, 2) (right figure) corresponding to a line source at (2, 2) with spectrum of the current $J_{e,z}(x, y, \omega)$ being a Gaussian pulse and a dielectric material going from (3, 1) to (4, 4) with a relative permittivity $\epsilon_r = 3$.

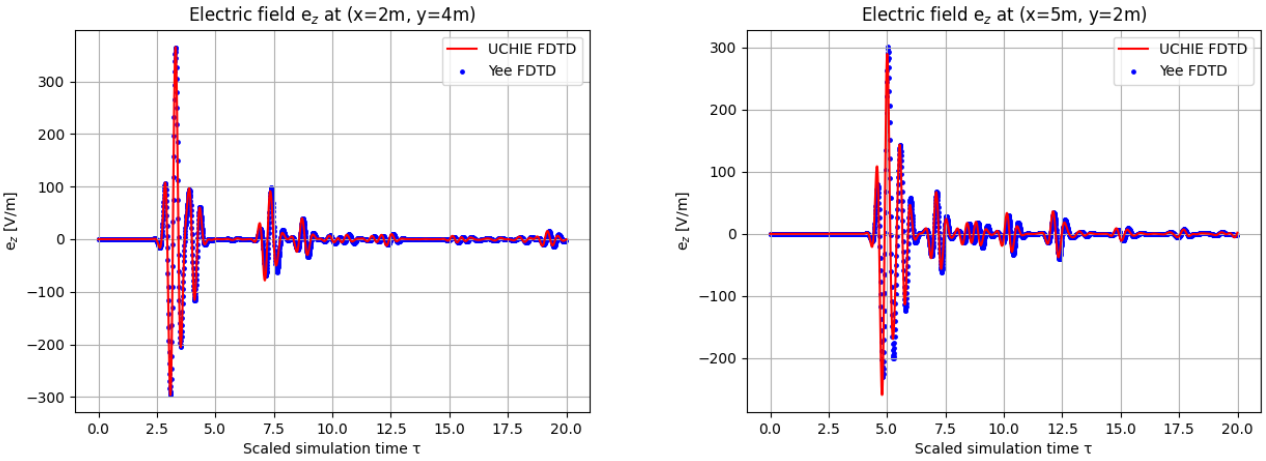

Figure 6: The electric fields $e_z(x, y, \omega)$ at (2,4) (left figure) and (5, 2) (right figure) corresponding to a line source at (2, 2) with spectrum of the current $J_{e,z}(x, y, \omega)$ being a modulated Gaussian pulse with a central frequency of 3.77 GHz and a dielectric material going from (3, 1) to (4, 4) with a relative permittivity $\epsilon_r = 3$.

2.3 Shielding by a conducting slab

The UCHIE FDTD scheme discussed above allows to simulate the scattering at and propagation through Drude media. In this section, the slab is assumed to be a conductor with $\gamma = 0$ and the shielding effectiveness SE as defined in eq. 33 is calculated for different parameters.

$$\text{SE} = 20\log_{10}\left(\left|\frac{e_{z,0}(x, y, \omega)}{e_z(x, y, \omega)}\right|\right) \tag{33}$$

with $e_z(x, y, \omega)$ the electric field on the discussed observation point and $e_{z,0}(x, y, \omega)$ the same field for free propagation.

2.3.1 Influence of slab conductivity

The first parameter to investigate is the conductivity of a slab that is infinite in the y-direction. The source was initialized with the specifications given in table 1. An observation point was placed at (4.5,2.5) and the width of the slab was chosen to be 1 m, going from x = 3m to x = 4m. Three simulations were done of a wave traveling through the slab, and for each simulation the SE was measured at the observation point. In each simulation, the slab had a relative permittivity and permeability of one, whilst the conductivity increased each time with one order of magnitude, having the values 2.72e-4 S/m, 2.72e-3 S/m, 2.72e-2 S/m.
The measured SE is shown in dB in figure 7. As expected, the SE is higher over the whole frequency range when the conductivity is increased. This is shown on the left side of the figure. The right side depicts the SE as a function of the conductivity at a frequency of 3.77 GHz and shows that the influence of the conductivity on the SE is exponential.

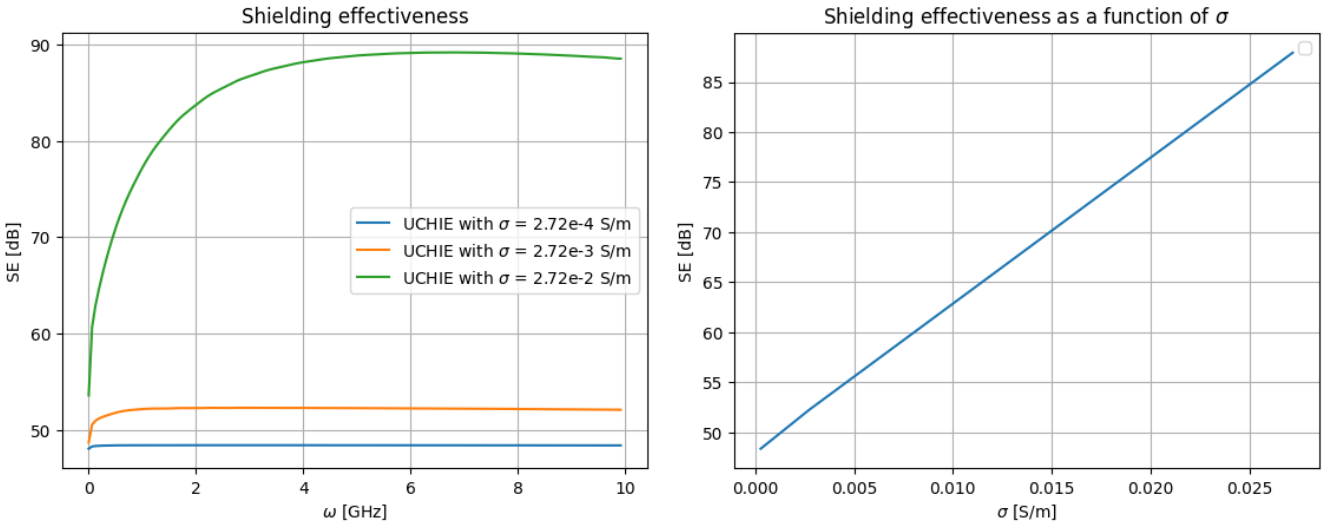

Figure 7: The SE as a function of frequency (left) and the SE as a function of the conductivity for a frequency of 3.77 GHz (right)

Example: WiFi through concrete walls This influence is well known in the attenuation of WiFi through concrete and reinforced concrete walls. The steel bars in the latter act like a Faraday cage and weaken the signal drastically. The UCHIE code can be used to simulate the WiFi signal at a central frequency of f=2.4 GHz propagating through a (reinforced) concrete wall of 0.5 meters thick. It must be noted that the electromagnetic parameters of concrete occupy an enormous range in orders of magnitude and are subject to a big list of specific parameters, but the general trend is simulated using a possible conductivity of $0.001\frac{S}{m}$ and $0.004\frac{S}{m}$ for concrete and reinforced concrete respectively as obtained from [1]. The result for a modulated Gaussian source with WiFi frequency as central frequency and an adequate bandwidth can be seen in figure 8

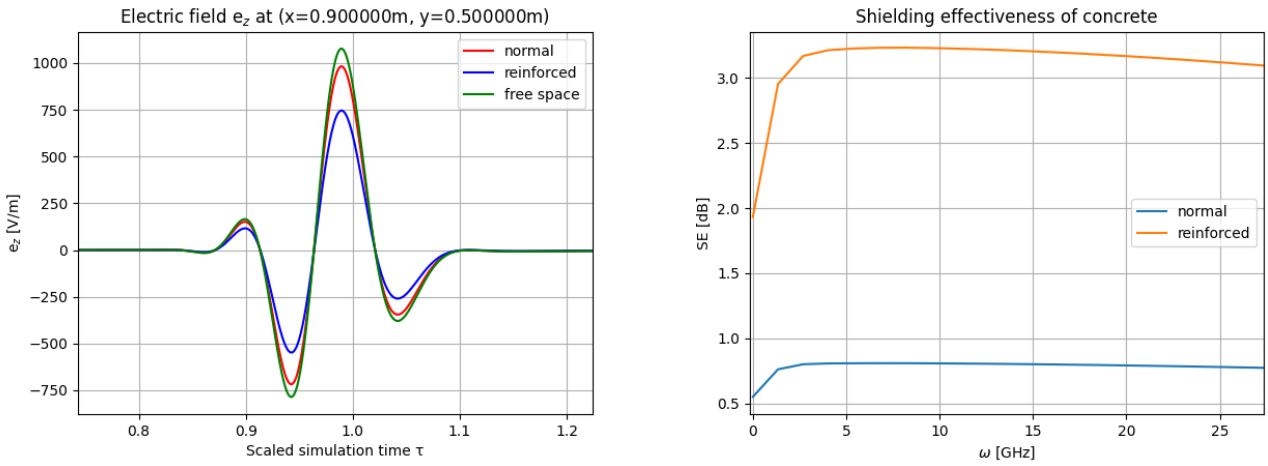

Figure 8: The electric field $e_z(x, y, \omega)$ and the SE at (0.9, 0.5) behind a (reinforced) concrete wall of 0.5m thick for a modulated Gaussian source with WiFi frequency as central frequency, a Gaussian width of 0.134ns and an amplitude of 2A located at (0.1, 0.5).

It is important to note that no frequency dependence was assumed for the conductivity of both concrete walls.

2.3.2 Influence of slab thickness

The next parameter is the slab thickness in the direction of propagation. For this experiment, three slab thicknesses were chosen: 0.5 m, 1 m and 1.5 m. For all three simulations, the slab starts at x = 3m and then extends to the right. The source specifications are shown in table 1 and an observation point is placed at position (4.8, 2.5) such that it lies outside the slab for all three slab thicknesses. The result is shown in figure 9 and also shows the expected behaviour, namely the SE increases when the slab is made thicker.

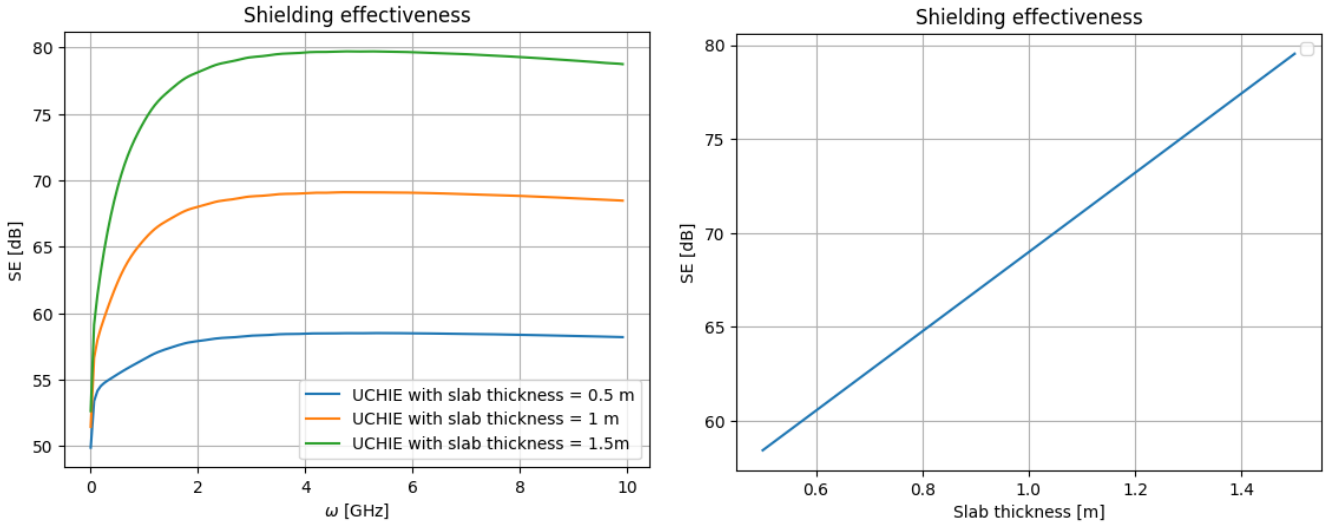

Figure 9: SE as a function of frequency (left) and as a function of slab thickness for a frequency of 3.77 GHz (right)

2.3.3 Skin effect

Instead of calculating the shielding effectiveness outside the slab, the Skin effect can be demonstrated near the exposed edge of a conducting slab. To avoid reflections when measuring the field at the exposed edge, the slab extends to infinity at the right side of the edge which is located at x = 3 m. A Gausian modulated source with a central frequency of 3.77 GHz, pulse width of 0.67e-9 s and amplitude 2 A was used at position (2, 2.5). The observation points are placed at (3.00, 2.5), (3.10, 2.5), (3.15, 2.5), (3.20, 2.5), (3.25, 2.5), (3.30, 2.5) and (3.35, 2.5) inside the slab. The slab has a relative permittivity and permeability of one and a conductivity of 0.272 S/m. Figure 10 shows on the left the shielding efficiency of the slab as a function of distance in the slab. This is a linear curve when the SE is plotted in dB, which is to be expected since the wave attenuates exponentially inside the slab. The right side of the figure shows the SE as a function of frequency at the different observation points. This shows that the skin effect is present over the whole frequency range of the source.

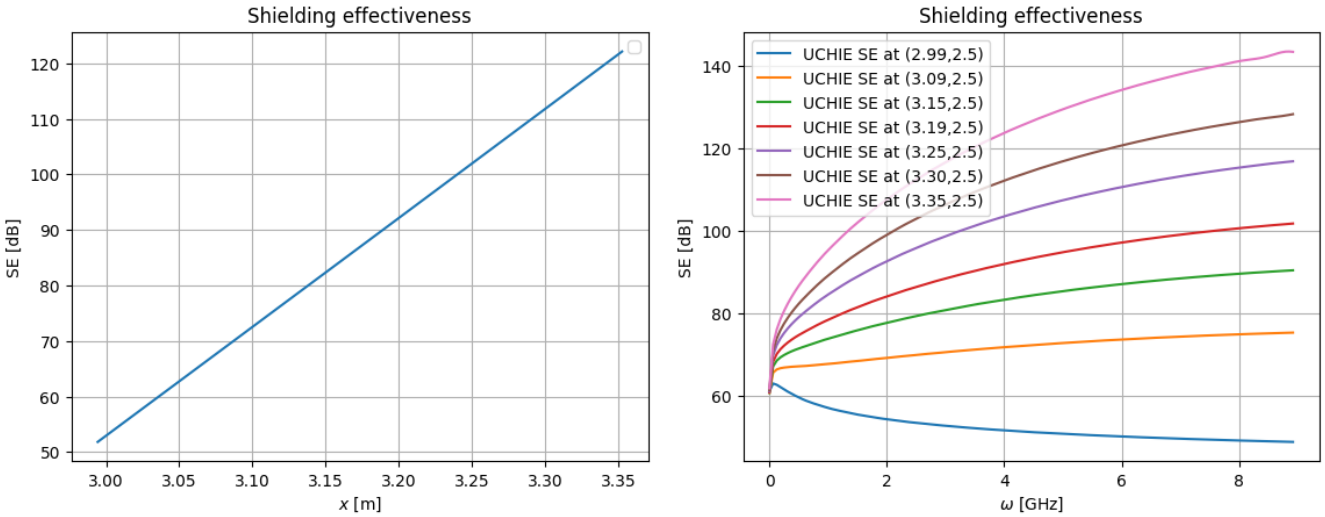

Figure 10: The SE as a function of distance in the slab (left figure) and The SE as a function of frequency for the different observation points in the slab (right figure)

2.4 Drude media

In Drude media, the conductivity is frequency dependent and has the form

$$\sigma(\omega) = \frac{\sigma_{DC}}{1 + \jmath\omega\gamma} \tag{34}$$

in the frequency regime. To identify the effect of this frequency-dependent conductivity, the shielding efficiency (SE) of a slab was measured for different values of γ. For this measurement, the source was placed at position (2,2.5), has an amplitude 2 A and is of the Gaussian modulated type with a central frequency of 3.77 GHz and a pulse width of 0.67e-9 s. The observation point was placed behind the slab at (4.5,2.5). The slab is 1 m wide ranging from 3 m to 4 m and goes from the bottom of the domain to the top so it can be seen as infinitely long. It has a relative permittivity and permeability of 1 and a DC conductivity of 0.0133 S/m. The different γ values used are: 0 s, 0.10e-9 s, 0.25e-9 s, 0.58e-9 s. Figure 11 shows the four different shielding efficiencies as a function of frequency. For a higher γ, the shielding efficiency decreases for higher frequencies. The reason for this is clear when looking at equation 34: when the product $\gamma\omega$ is large enough, the overall conductivity will go to zero. The larger frequencies will thus be less attenuated.

	J_0	Type	Gaussian width	Central frequency	Position
Source parameters	2 A	Gaussian modulated	0.67e-9 s	3.77 GHz	(2, 2.5)

Table 1: The source specifications used in some simulations

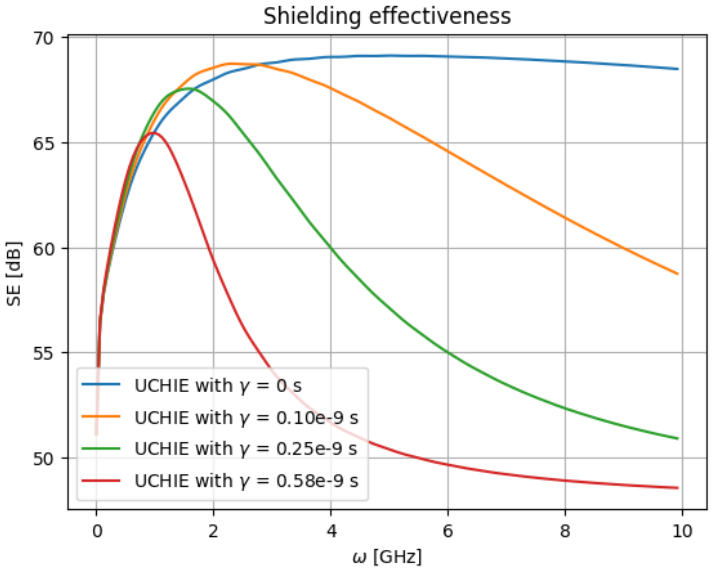

Figure 11: Shielding efficiency for $\gamma = 0\ s^{-1}$, 0.10e-9 s^{-1}, 0.25e-9 s^{-1}, 0.58e-9 s^{-1}

3 Conclusion

The UCHIE FDTD scheme was compared with the analytical solution of a wave coming from a line source in 2-D. This comparison showed that the scheme is able to reproduce the analytical solution with a sufficient accuracy. To obtain a correct amplitude and phase of the frequency response for higher frequencies, the bandwidth of the line source should be expanded.
One advantage of the UCHIE scheme as seen in figure 1 over the Yee FDTD is the possibility to place the vertical material boundaries between the collocated fields. This way interpolation and differentiation in the x-direction does not require the interpolation of the different material parameters and the sharp boundary can be resolved with perfect precision. This advantage is not present in the y-direction.
The downside of the collocation in the x-direction of the UCHIE scheme is that it is partially implicit. As a result, a matrix inversion is needed when updating the fields. This causes the scheme to be sufficiently slower than Yee FDTD, making the statement 'there is no such thing as a free meal' true in the sense that a trade-off is made between accuracy and speed. Simulating high frequencies requires small grid steps, which make the matrix as defined in 26 large and therefore make the UCHIE code slower.

References

[1] J.-F. Lataste. "12 - Electrical resistivity for the evaluation of reinforced concrete structures". In: *Non-Destructive Evaluation of Reinforced Concrete Structures*. Ed. by Christiane Maierhofer, Hans-Wolf Reinhardt, and Gerd Dobmann. Vol. 2. Woodhead Publishing Series in Civil and Structural Engineering. Woodhead Publishing, 2010, pp. 243–275. ISBN: 978-1-84569-950-5. DOI: https://doi.org/10.1533/9781845699604.2.243. URL: https://www.sciencedirect.com/science/article/pii/B9781845699505500129.